Rigid boundary conditions for staggered-grid modelling

Zaiming Jiang, John C. Bancroft, and Laurence R. Lines

ABSTRACT

Staggered-grid modelling methods have been shown previously to be more accurate than non-staggered grid schemes when liquids are involved inside the subsurface models. This report shows that the staggered-grid modelling can also accurately simulate seismic activities when rigid boundaries are involved.

The rigid boundary is discussed from both mathematical and numerical perspectives. First, formulas about rigid boundary reflections are mathematically derived and qualitatively interpreted. Specifically, seismic reflection amplitude and polarity changes at wide incident angles are discussed. Second, a finite-difference implementation of the rigid boundary conditions is designed within a staggered-grid modelling scheme and the modelling results are presented. It is shown that the numerical modelling results accurately match the mathematical derivations and qualitative interpretations.

The validity of the implementation method of the rigid boundary conditions within a staggered-grid modelling scheme is also proven.

INTRODUCTION

When one develops software applications of algorithms of numerical wave modelling, the question needs to be answered: is the modelling done correctly? One needs to answer this question with the seismic source, the free surface, the internal physical boundaries, such as point diffractors and layered reflectors at different angles, and the computational boundaries on the left, right, and bottom of subsurface models.

In the case of computational boundaries on the left, right, and bottom of 2D subsurface models, it is desirable that there are no boundary reflections at all, or the boundary reflections are attenuated to a very low level compared to the physical reflections inside the subsurface models. Thus, over the past 40 years, people have developed various boundary conditions, such as absorbing boundary conditions (Engquist and Majda, 1977; Clayton and Engquist, 1977), nonreflecting boundary conditions (Cerjan, Kosloff, Kosloff, and Reshef, 1985), transparent boundary conditions (Long and Liow, 1990), perfectly matched layer boundary conditions (Collino and Tsogka, 2001), and combined boundary conditions (Jiang, Bancroft, and Lines, 2010).

The importance of a rigid boundary lies in at least two aspects. First, it exists in theory and represents a logical end point within the physical world. Second, it is important for comparison to the various computational boundary condition methods.

It has been shown that the staggered-grid scheme deals with a liquid-solid interface without the need for special treatment, which is not the case for non-staggered grid schemes (Virieux, 1986; Levander, 1988; Stephen, 1988). This report shows that the staggered-grid modelling can also accurately simulate seismic activities when rigid boundaries are present in subsurface models.

This report discusses rigid boundary reflections from two different perspectives.

Firstly, formulas about rigid boundary reflections are mathematically derived and qualitatively interpreted. The objective is to answer a question: what are the reflections from a rigid boundary? Specially, are there going to be both reflections of compressional waves and shear waves, or only compressional waves, when a compressional wave travels inside a solid medium and hits a rigid boundary? If both waves are reflected off the rigid boundary, what should be the amplitudes and polarities?

Secondly, a finite-difference implementation method of rigid boundary conditions in a staggered-grid scheme is presented and the numerical modelling results are shown.

It is shown that the modelling results accurately match the mathematical derivations and qualitative interpretations. Thus, the correctness of the algorithm of rigid boundary conditions within a staggered-grid system is confirmed.

REFLECTIONS FROM A RIGID BOUNDARY IN THEORY

Theoretically, what are the reflections off a rigid boundary?

Consider the P-SV case shown in Figure 1. An incident P wave striking a boundary of media 1 and 2 produces reflected and transmitted P and SV waves. The boundary conditions are governed by the four Zoeppritz equations, which contains the following two equations for horizontal and tangential components of displacement (Krebes, 2006).

$$(A_I + A_R)sin\theta_1 + (B_I + B_R)cos\emptyset_1 = A_T sin\theta_2 + B_T cos\emptyset_2 \qquad (1a),$$

$$(A_I - A_R)cos\theta_1 - (B_I - B_R)sin\emptyset_1 = A_T cos\theta_2 - B_T sin\emptyset_2 \qquad (1b),$$

where A and B, respectively, represent amplitudes of the P and SV waves; I, R, and T, the incident, reflected, and transmitted waves; and θ and Φ, respectively, represent P and SV wave angles.

Waves striking a rigid boundary condition produce no motion on the boundary. Thus, the boundary conditions for the rigid boundary are: the normal and tangential components of displacement must be zero (Krebes, 2006).

Consider a special case that there is only an incident P wave, i.e., there is no incident SV wave. There are no transmitted waves beyond the rigid boundary, so the boundary conditions in equation (1) can be re-written as

$$(A_I + A_R)sin\theta + B_R cos\emptyset = 0, \qquad (2a)$$

$$(A_I - A_R)cos\theta + B_R sin\emptyset = 0, \qquad (2b)$$

where media subscripts are dropped, since only medium 1 is involved.

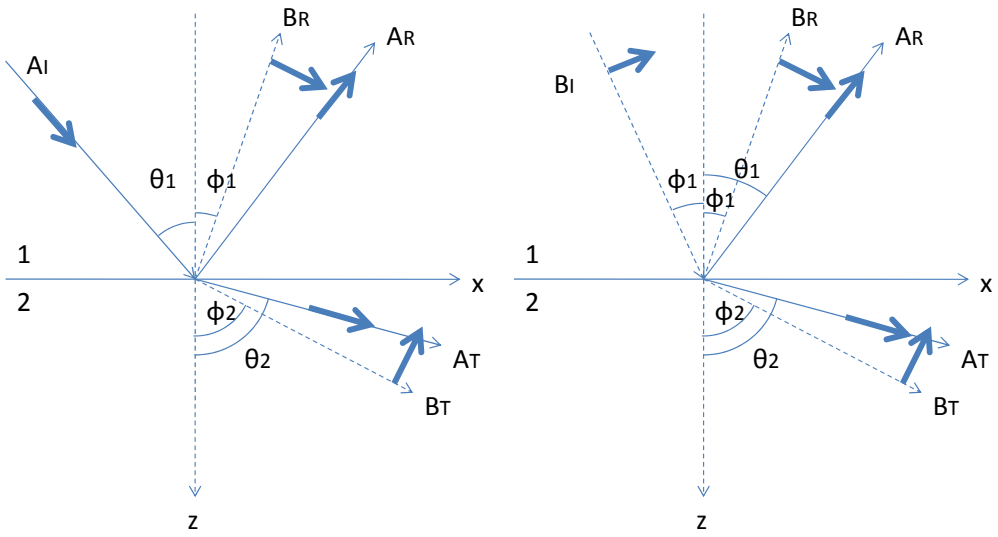

FIG. 1. Reflection and transmission of an incident P (left) and SV (right) wave. A and B, respectively, represent amplitudes of P and SV waves; I, R, and T, respectively, represent incident, reflected, and transmitted waves; The boldface arrows define the virtual positive directions of particle motion (adapted from Krebes, 2006).

Solving for the reflected P and SV waves yields

$$A_R = \frac{cos\theta cos\emptyset - sin\theta sin\emptyset}{cos\theta cos\emptyset + sin\theta sin\emptyset} A_I, \tag{3a}$$

$$B_R = -\frac{2sin\theta cos\theta}{cos\theta cos\emptyset + sin\theta sin\emptyset} A_I. \tag{3b}$$

Using the trigonometric addition formulas yields

$$A_R = \frac{\cos(\theta+\emptyset)}{\cos(\theta-\emptyset)} A_I, \tag{4a}$$

$$B_R = -\frac{\sin(2\theta)}{\cos(\theta-\emptyset)} A_I. \tag{4b}$$

These equations tell us that

1. The incident P wave energy is all reflected as P wave energy, i.e., there is no reflected SV wave, when an incident P wave travelling inside a solid medium strikes a rigid boundary with an incident angle equal to zero. There are both P and SV wave reflections when the incident angle is greater than zero.

2. For the vertical displacement, there is a polarity reversal for the P wave reflections compared to the incident P wave when the incident angle is such that (θ + Φ) is less than 90 degrees. This is determined by not only the reflection coefficient $R_{PP} = A_R/A_I$ given by equation (4a), but also by the polarity vector (the boldface arrow in Figure 1). The amplitude of the reflected P wave becomes weaker when the incident angle becomes greater, until the reflected P wave disappears when the incident angle is such that (θ + Φ) is equal to 90 degrees. Denoting the unique P-wave incident angle and S-wave

reflection angle as θ_{UN} and Φ_{UN}, by applying Snell's law, these angles can be decided as

$$\theta_{UN} = \arctan\left(\frac{V_p}{V_s}\right), \quad (5a)$$

$$\emptyset_{UN} = \arctan\left(\frac{V_s}{Vp}\right). \quad (5b)$$

When the incident angle is even greater such that (θ + Φ) is greater than 90 degrees, the reflected P wave appears again, but there is no polarity reversal compared to the incident P wave.

3. For the horizontal vertical of the reflected P wave, similar conclusions can be drawn, but the polarities are different. When the incident angle of the incident P wave is small enough, there will be no polarity reversal for the reflected P wave, compared to the incident P wave. Then there will be a polarity change in the reflected P wave when the incident angle reaches θ_{UN}.

4. There is no reflected SV wave when the incident P wave is vertically incident upon a rigid boundary. The reflected SV wave appears when the incident angle is greater than zero.

The above interpretations can be used to judge the validity of an algorithm of rigid boundary conditions in numerical wave modelling.

RIGID BOUNDARY CONDITIONS IN STAGGERED-GRID MODELLING

Special implementation of rigid boundary conditions in staggered-grid modelling

A staggered-grid scheme with velocity / stress and time splitting, which was presented by Virieux (1986), is used to numerically model the elastic waves. The particle velocity numerical nodes are illustrated in Figure 2. The indexes of the lines of horizontal particle velocity nodes are from 0 to *J-1* for the horizontal particle velocities, and from *1/2* to *J-1/2* for the vertical particle velocity nodes.

The natural assumption for the rigid boundary conditions is to set the boundary particle velocities to zero, i.e., set the values on the nodes on line *J-1* and *J-1/2* in Figure 2 to zero, but this turns out to be false. This conclusion is drawn from the fact that there are only P wave reflections off the boundary resulting in the numerical modelling experiment. Why does this implementation of rigid boundary conditions fail? The reason is that this method does not guarantee the horizontal particle velocities on the boundary (line *J-1/2*) to be zero.

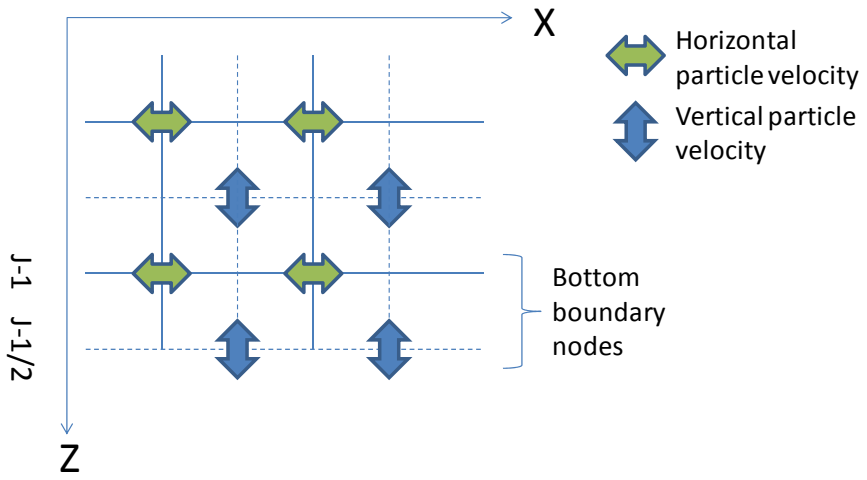

FIG. 2. A staggered-grid scheme with velocity / stress and time splitting. Only particle velocity nodes are shown.

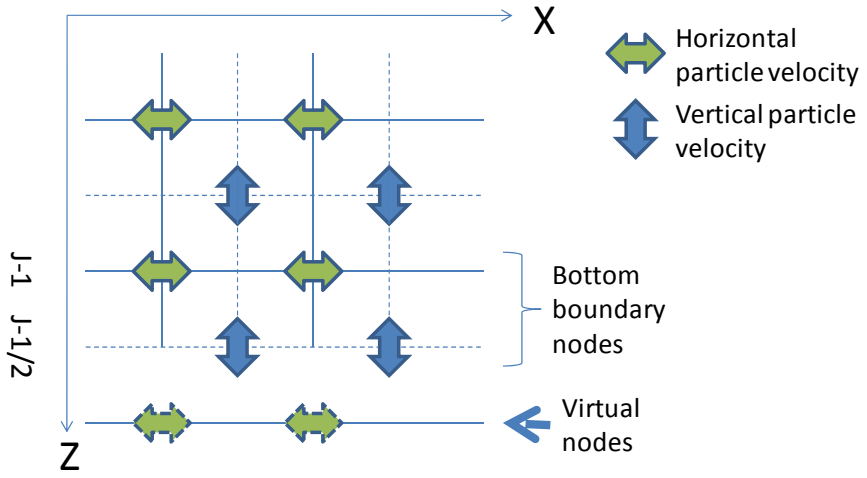

FIG. 3. For the bottom boundary a virtual line of nodes is put on the line *J*, outside of the subsurface model.

Taking the line *J-1/2* to be the rigid boundary, in addition to the values of vertical particle velocities on this line being set to zero, one should also assure that the horizontal particle velocities on this line to be equal to zero although there are no real numerical nodes on this line. If a virtual line of nodes is put on the line *J*, and the values on the virtual line are set anti-symmetric to those on the line *J-1* (Figure 3), i.e.,

$$U_J = -U_{J-1}, \tag{6}$$

where *U* denotes the vertical particle velocity, then the values on the boundary line *J-1/2* would be guaranteed to be zero by the central finite difference:

$$U_{J-\frac{1}{2}} = \frac{1}{2}(U_J + U_{J-1})=0. \quad (7)$$

Numerical modelling experiment

A 2D subsurface model is built to check the algorithm. The subsurface is 5000 meters in length and 1000 meters in depth, and it is a homogeneous medium. The space steps on both horizontal and vertical directions are the same: 1.25m. The P wave velocity is 3000 m/s and the density is estimated by Gardner's relationship. Then the S wave velocity is calculated to be 1732 m/s by assuming the Poison's ratio to be 0.25. After the velocity and density parameters are decided, the Lame coefficients are calculated and then used with the density data in numerical modelling.

An explosive source is placed at the centre of the surface. The source consists of four zero phase Ricker wavelets with peak frequency equal to 40 Hz.

The time step of modelling is 0.00016s and the number of total time steps is 5500, which makes the total time of modelling to be 0.88s.

Modelling results

Modelling snapshots of the centre shot are shown in Figure 4 and 5. Figure 4 shows the vertical component and Figure 5 shows the horizontal one. There are six snapshots for each component, and the snapshots are shown in time order.

In the snapshots of time 0.288s, a P wave, a SV wave, and down-going header waves are traveling outwards from the seismic source, which is at the surface centre. On the surface, Rayleigh waves, which are slower than the SV wave, are also observed.

In the snapshots of time 0.4s, the P wave strikes the bottom boundary, and reflections are produced although the reflections are not clearly distinguishable.

At times 0.512s and 0.624s the reflected P and SV waves are clearly distinguishable. The polarity reversal of the vertical component of the reflected P wave, compared to the incident P wave, can be observed. With the incident angles of the P wave on the bottom boundary becoming greater and greater, the P wave reflection becomes weaker and weaker. Spherical spreading is one cause of the amplitude attenuation, but the main cause is the incident angle change.

At time 0.736s, the P wave reflected off the bottom boundary becomes very weak and seems to have disappeared. In fact, for this specific medium, in which P-wave and S-wave velocities are, respectively, 3000 m/s and 1732 m/s, according to equations (5a) and (5b), when the incident angle θ is equal to 60 degrees, the PS reflection angle Φ is 30 degrees, and in turn, ($\theta + \Phi$) is equal to 90 degree. Thus, the amplitude of the reflected P wave is zero when the incident angle θ is equal to 60 degrees in this specific medium.

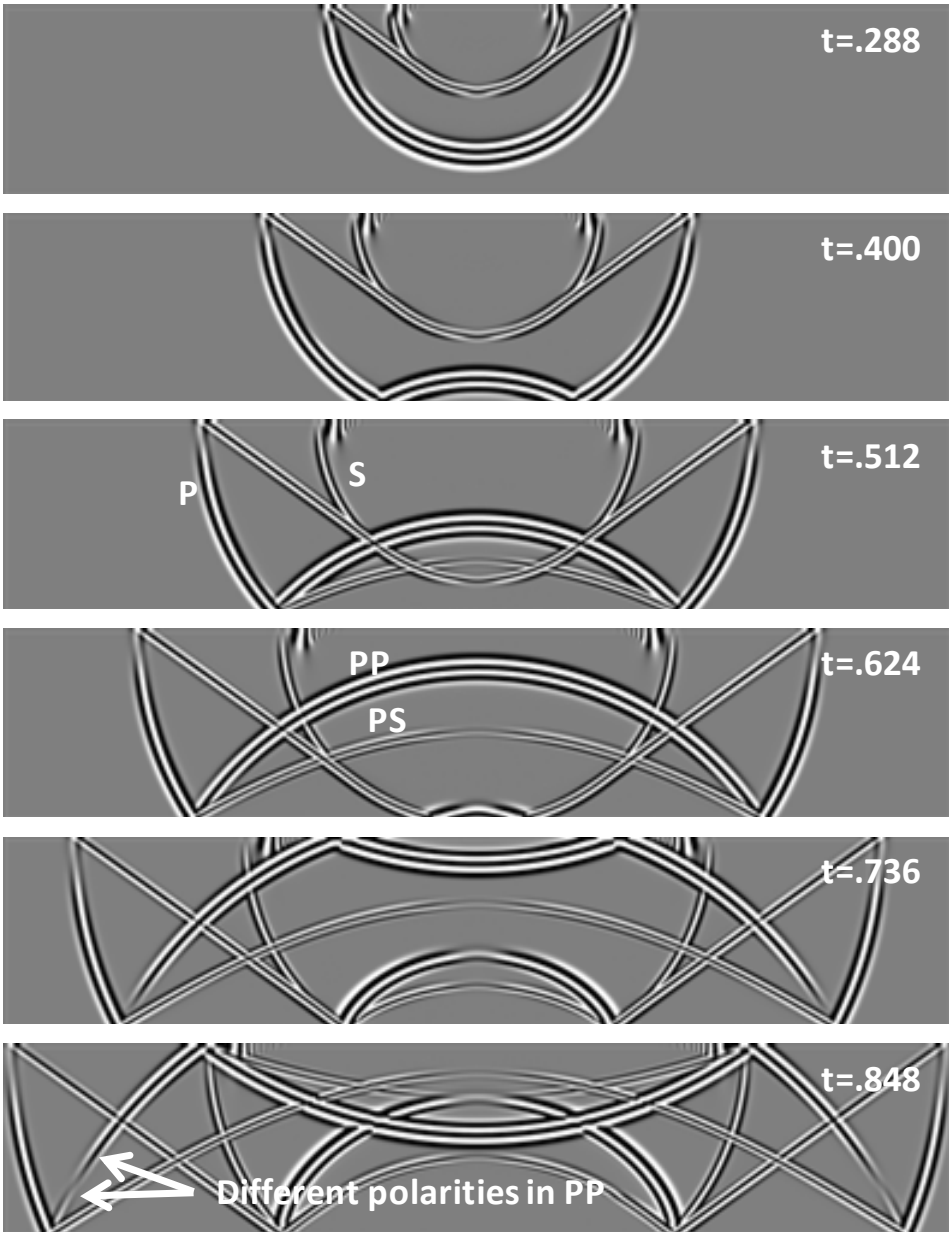

FIG. 4. Vertical component snapshots of particle velocity data in time order. The source is at the centre of the surface, and the bottom is a rigid boundary. The unit for time is second. PP and PS, respectively, represents the P and SV wave reflections from an incident P wave.

At time 0.848s, the P wave reflection has reappeared with a reversed polarity, which leads to two different polarities observable on the same wave front of the P wave reflection, which was predicted mathematically.

The above observations accurately match the mathematical derivations and qualitative interpretations, which are described in the previous section.

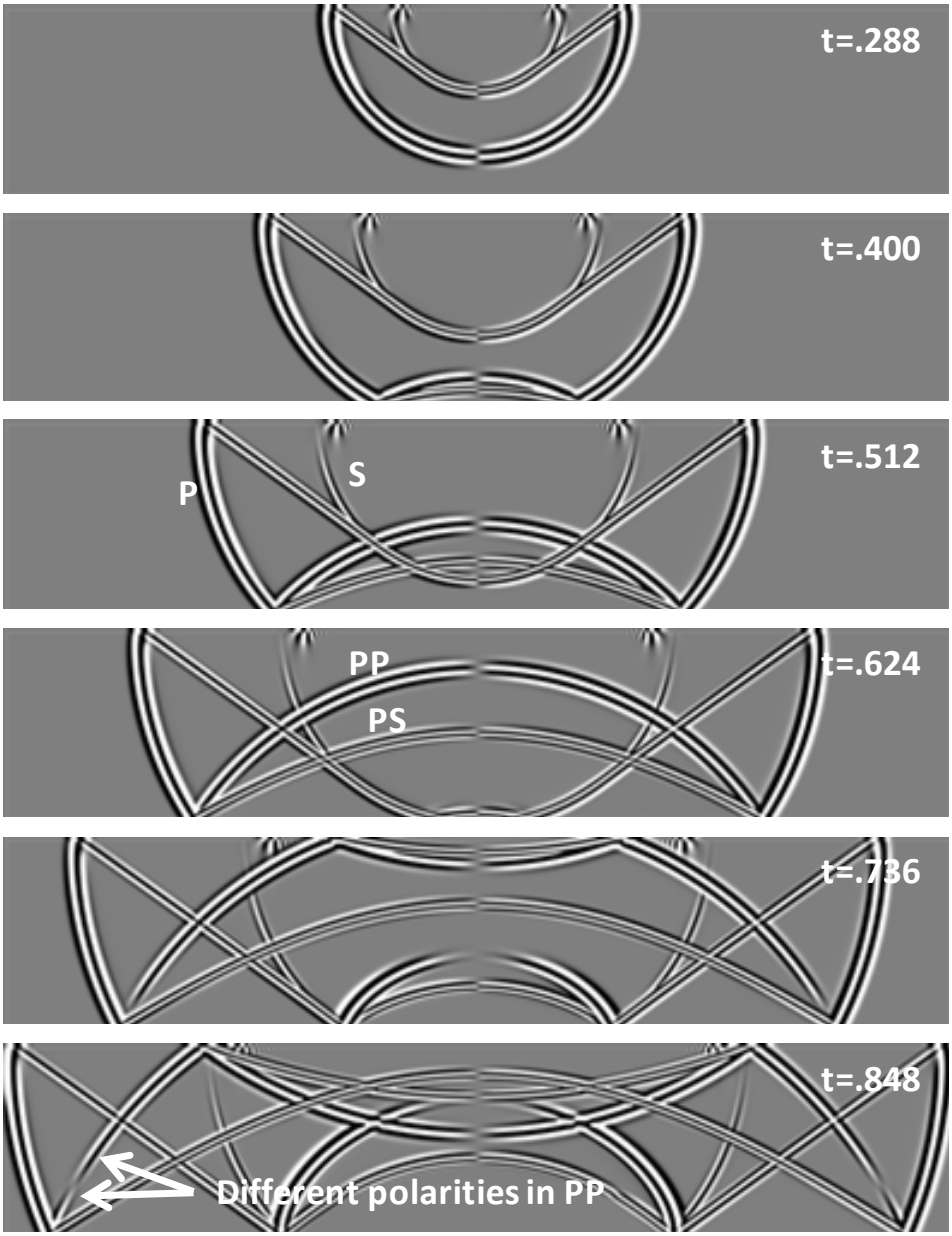

FIG. 5 Horizontal component snapshots of particle velocity data in time order.

CONCLUSIONS

Formulas describing the rigid boundary reflections are derived from the two Zoeppritz equations about horizontal and vertical displacements. It is predicted that (1) there are both P and SV wave reflections when a P wave traveling in a solid medium strikes a rigid boundary at an incident angle other than zero; (2) the amplitudes of P and SV wave reflections vary with the incident angle; and (3) the P wave reflection changes polarity at a certain wide incident angle.

Numerical rigid boundary for elastic modelling should be so designed that at the boundary the finite-difference estimates of both the horizontal and the vertical particle

velocities (or displacements) are zero. The method presented in this report is proven to be valid, since the modelling results accurately match the mathematical analysis.

ACKNOWLEDGEMENTS

We thank the sponsors of CREWES for their continued support. The first author is thankful to Dr. Edward S. Krebes for direction on seismic theory and Dr. Peter M. Manning for discussions on numerical modelling.

REFERENCES

Cerjan, C., Kosloff D., Kosloff, R., and Reshef, M, 1985, A nonreflecting boundary condition for discrete acoustic and elastic wave equations, Geophysics, 50, 705-708.

Clayton, R., and Engquist, B., 1977, Absorbing boundary conditions for acoustic and elastic wave equations, Bulletin of the Seismological Society of America, 67, 1529-1540.

Engquist, B. and Majda, A.,1977, Absorbing boundary conditions for numerical simulation of waves, Proc. Natl. Acad. Sci. USA, 74, 1765-1766.

Collino, F., and Tsogka, C., 2001, Application of the perfectly matched absorbing layer model to the linear elastodynamic prolem in anisotropic heterogeneous media, Geophysics, 66, 294-307.

Jiang, Z., Bancroft, J.C., and Lines, L.R., 2010, Combining absorbing and nonreflecting boundary conditions for elastic wave simulation, SEG International Exposition and Eightieth Annual Meeting, Denver, Colorado.

Krebes, E.S., 2006, Seismic theory and methods: Course notes.

Levander, A. R., 1988, Fourth-order finite-difference P-SV seismograms: Geophysics, 53, 1425–1436.

Long, L.T., and Liow J.S., 1990, A transparent boundary condition for finite-difference wave simulation, Geophysics, 55, 201-208.

Stephen, R.A., 1988, A review of finite difference methods for seismo-acoustic problems at the sea floor: Reviews of Geophysics, 26, 445-458.

Virieux, J., 1986. P-SV wave propagation in heterogeneous media: velocity-stress finite-difference method, Geophysics, 51, 889--901.